Available online at www.sciencedirect.com
SCIENCE DIRECT
Journal of Power Sources 155 (2006) 264–271
JOURNAL OF POWER SOURCES
www.elsevier.com/locate/jpowsour

Effect of gas flow-field design in the bipolar/end plates on the steady and transient state performance of polymer electrolyte membrane fuel cells

Atul Kumar [a,*], Ramana G. Reddy [b]

[a] *Houston Advanced Research Center, Clean and Renewable Energy, 4800 Research Forest Drive, The Woodlands, TX 77381, USA*
[b] *Department of Metallurgical and Materials Engineering, The University of Alabama, Box 870202, Tuscaloosa, AL 35487-0202, USA*

Received 1 April 2005; received in revised form 7 May 2005; accepted 10 May 2005
Available online 11 July 2005

Abstract

In this work the effect of gas flow-field design in the bipolar/end plates on the steady and transient state performance of the polymer electrolyte membrane fuel cell (PEMFC) is presented. Simulations were performed with different flow-field designs, viz. (1) serpentine; (2) parallel; (3) multi-parallel; and (4) discontinuous. The steady-state voltage at fixed current density of 5000 A m^{-2} was highest for discontinuous design. For studying the transient response, the average current density was increased suddenly from 5000 to 8000 A m^{-2}. It was seen that when the load level was increased, the voltage level suddenly dropped and then with time leveled off to a value slightly higher than the dropped value. This time for serpentine, parallel, multi-parallel and discontinuous flow-fields were 9.5, 7.5, 8.0 and 16.5 s, respectively. While it was seen that the steady-state performance of the discontinuous type of design was the maximum, its transient response was slow. On the other hand in case of parallel type of design the steady-state performance was low, but the transient response was high. The multi-parallel design offers a unique advantage of both of these properties, viz. high steady-state performance with good transient response, and therefore should perform better than the other designs chosen in this study.

Keywords: Polymer electrolyte membrane fuel cell; Membrane electrode assembly; Bipolar plate

1. Introduction

The polymer electrolyte membrane fuel cell (PEMFC) is seen as a system of choice for automotive applications due to several advantages that this type of fuel cell offers over the other types (alkaline fuel cell, phosphoric acid fuel cell, molten carbonate fuel cell and solid oxide fuel cell). PEMFCs operate at lower temperature (∼80 °C), thereby allowing for faster startups and immediate response to changes in demand of power. Also these systems are environmentally friendly and hence suited best for automobile applications.The PEMFC consists of an anode, cathode and a proton exchange membrane (electrolyte). The electrolyte membrane is sandwiched in between anode and cathode. Pure hydrogen or hydrogen rich reformate gas is passed onto the anode side, wherein the hydrogen breaks into protons (H^+) and electrons (e^-). These H^+ ions pass through the electrolyte (protonic conductor) onto the cathode side, while the electron follows through the outer circuit generating electricity. Air or oxygen is the oxidant on the cathode side. The oxygen molecule combines with these H^+ ions and electrons on the cathode side to generate the by-product water and heat. The electrochemical reactions for the process can be represented as:

$$\text{anodic}: \quad H_2 \rightarrow 2H^+ + 2e^- \tag{1}$$

* Corresponding author. Tel.: +1 281 364 6009; fax: +1 281 363 7935.
E-mail address: akumar@harc.edu (A. Kumar).

0378-7753/$ – see front matter © 2005 Elsevier B.V. All rights reserved.
doi:10.1016/j.jpowsour.2005.05.006

Nomenclature

a_k	activity of water at interface k
A_{cv}	specific area of control volume ($m^2\ m^{-3}$)
$D_{i,j}$	binary mass diffusion coefficient of component i in component j ($m^2\ s^{-1}$)
E	theoretical cell voltage (V)
F	Faradays constant ($C\ eq^{-1}$)
F_{stk}	compaction force of the stack ($N\ m^{-2}$)
I_0	exchange current density for the oxygen reaction ($100\ A\ m^{-2}$)
I	current density ($A\ m^{-2}$)
I_L	limiting current density ($A\ m^{-2}$)
J_k	diffusion flux of species k ($kg\ m^{-2}\ s^{-1}$)
k_p	permeability of water in membrane (m^2)
m_k	mass fraction of species k
M_k	molecular weight of species k (kg)
$M_{m,dry}$	equivalent weight of dry membrane ($kg\ mol^{-1}$)
p_k	partial pressure of species k (Pa)
P	pressure (Pa)
$P^{sat}_{w,k}$	Saturation vapor pressure of water at 'k' interface
R	universal gas constant ($J\ mol^{-1}\ K^{-1}$)
R^k_{CR}	contact resistance of material k (ohms)
R_{memb}	resistance of membrane (ohms)
S_k	source term for species k ($kg\ m^{-3}\ s^{-1}$)
t_m	polymer membrane thickness (m)
T	temperature (K)
$\vec{v}$	velocity vector ($m\ s^{-1}$)
V	actual cell voltage (V)

Greek symbols

α	net water flux per H^+
β	permeability of the electrodes (m^2)
η_{act}	activation polarization (V)
η_{ohm}	ohmic polarization (V)
η_{conc}	concentration polarization (V)
ρ	density ($kg\ m^{-3}$)
$\rho_{m,dry}$	density of dry electrolyte membrane ($kg\ m^{-3}$)
σ_m	membrane conductivity ($mho\ m^{-1}$)
μ_k	viscosity of species k ($Pa\ s^{-1}$)

$$\text{cathodic}: \quad 1/2O_2 + 2H^+ + 2e^- \rightarrow H_2O \tag{2}$$

$$\text{net-reaction}: \quad H_2 + 1/2O_2 \rightarrow H_2O + \text{Heat} + \text{Electricity} \tag{3}$$

In spite of the presence of fuel cell technology for over 150 years, some technical issues exist that prohibit the wide scale commercialization of these fuel cells. Some of these issues related in particular to PEMFC are: (1) high cost of PEMFC components; (2) catalyst poisoning by CO concentration in the fuel; (3) water management in large stacks; (4) proton exchange membrane operating temperature limits; and (5) cell stack life. The biggest challenge of these is the reduction in cost of the fuel cell stack, which is mainly ascribed to the bipolar/end plates and precious metal catalysts. Additionally, the cost can be decreased by the optimization of the fuel cell process. Several models have been developed for optimization of the electrochemical kinetics of the process. However, little attention has been on the optimization of the flow-field design in the bipolar/end plates of the fuel cell [1–3]. For example, Kumar and Reddy showed in their work that optimum dimensions of the channels in the flow-field exist where the fuel cell gives the maximum performance [3]. Most of the existing models are developed under steady-state conditions and assume the flow-field to be serpentine type. This work therefore concentrates on the effect of the flow-field design on the steady state and the transient behavior of the fuel cell. Several flow-field designs, viz. (1) serpentine; (2) parallel; (3) multi-parallel; and (4) discontinuous were studied for their steady state and transient performance of the fuel cell.

2. Model development

The current model is a three-dimensional single-phase transient isothermal numerical mass-transfer unified model for PEMFC. The steady-state performance is just a special case where all the time dependent terms in the governing transport equations would be nullified. Numerical predictions of the voltage would be made for changing load (current) levels. The transient behavior would be studied for different flow-field designs (serpentine, parallel, multi-parallel and discontinuous) in bipolar/end plates of the fuel cell. Also, the steady-state performance would be calculated for each of the designs and results would be compared. The overall performance of the flow-field design would be judged based on the steady state and transient behavior of the fuel cell. This would help in finding the best possible flow-field design for the bipolar/end plates of the fuel cell. The detailed step-wise development of the unified model is discussed in following sections.

2.1. Problem domain

The simulation domain consists of cathode and anode flow-fields corresponding to the cathode and anode sides of the fuel cell, respectively, separated by the membrane electrode assembly (MEA) in between. The MEA consists of cathode and anode porous gas diffusion layer and catalyst layer, on each side of the membrane. The active area of the domain was a square of side 7.62 cm (3 in.). Fig. 1 shows the detailed cross-section (X–Z section) of the problem domain for this model. Each of the layers is marked by a separate zone. These are: cathode flow-field; cathode diffusion layer; cathode catalyst layer on the cathode side; anode flow-field; anode diffusion layer; and anode catalyst layer on the anode side of the fuel cell. The cathode and anode flow-field were

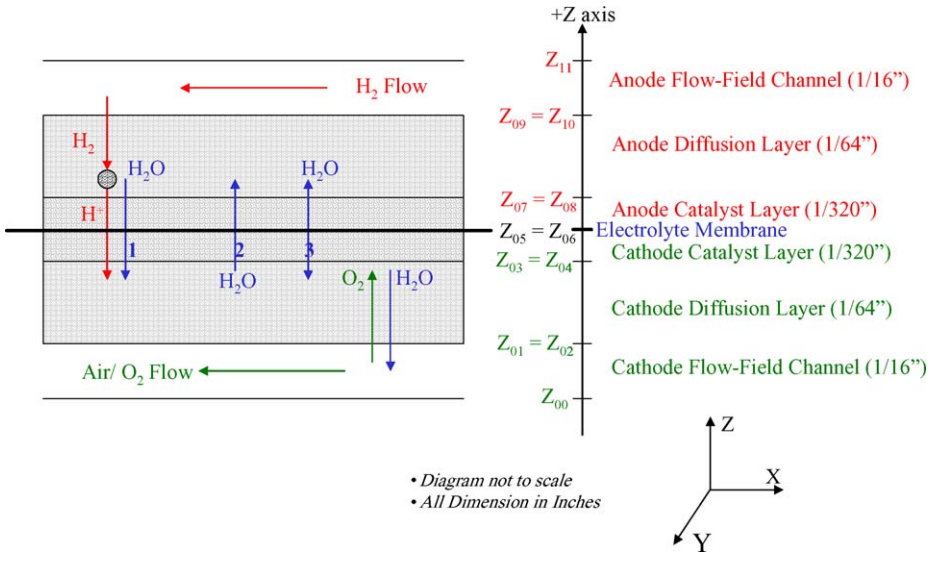

Fig. 1. Schematic of polymer electrolyte membrane fuel cell cross-section (*X–Z* section) showing different zones and transport of species across these zones.

essentially the machined channels in the bipolar/end plates. These help to distribute the reaction gases uniformly over the reaction surface. In this work four different flow-field designs were studied. Fig. 2(a–d) shows the schematic (*X–Y* section) for all of these flow-field designs. The dimension of the channel width, land width, and channel depth was 1.587 mm (1/16 in.). The cathode and anode gas diffusion layers were the electrodes made with porous carbon cloth that helps to diffuse the reactant gases from the bipolar/end plate flow-field channels towards the reaction catalyst layer, and also diffusion of byproduct water from the reaction site back to the flow-field channels. The catalyst layer on both the cathode and anode sides consists of platinum coating, and is essentially where all the electrochemical reactions take place.

We consider four different species in our model, viz. hydrogen (H_2), oxygen (O_2), nitrogen (N_2), and water (vapor) (H_2O). Each of the species flux was tracked in the domain through the control volume technique, which was used in solving the model. For example, consider the hydrogen species. The hydrogen from the anode flow-field channels is transported through the anode diffusion layer towards the anode catalyst layer. The catalyst action dissociates the

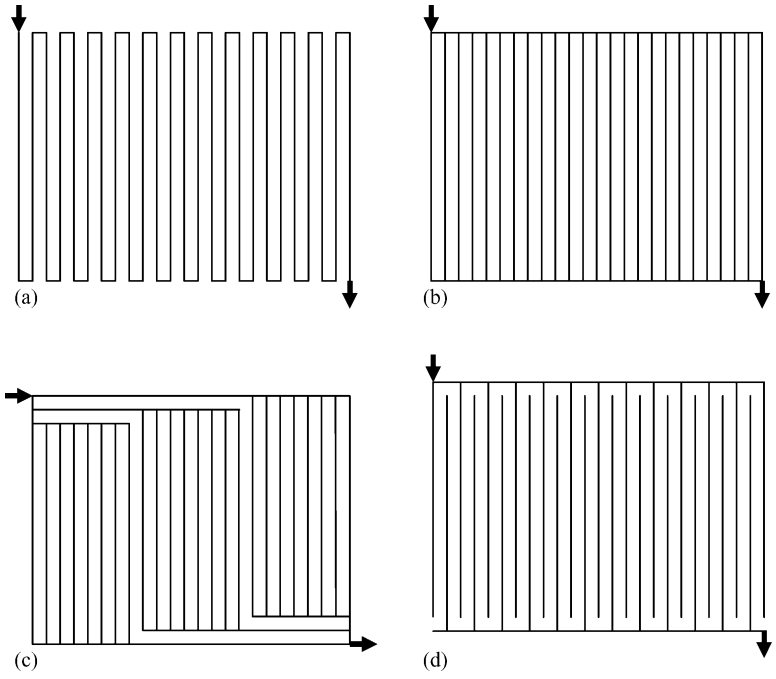

Fig. 2. Schematic of (a) serpentine; (b) parallel; (c) multi-parallel; and (d) discontinuous flow-field designs used in simulations.

hydrogen molecule to protons and electrons according to the Eq. (1). The protons generated above will transfer through the electrolyte membrane onto the cathode side, wherein they combine with oxygen to generate water. So there is a consumption of hydrogen and oxygen species on the anode and the cathode side, respectively, and generation of water species on the cathode side. Similarly other species were tracked in the domain.

2.2. Model assumptions

The following assumptions were used in developing the unified model for PEMFC.

(1) Stationary conditions exist in the single-cell PEMFC stack. Also, the effect of gravity was neglected.
(2) Based on the Reynolds number calculation ($Re \sim 500$) the flow in the fuel cell domain is laminar. Hence, all the transport equations were formulated for the laminar regime behavior.
(3) The proton exchange membrane was considered as a solid wall in the development of the model, and transport of species (protons and water molecules) across the membrane was taken into account through the incorporation of source terms in the transport equations.
(4) The gas diffusion layer and the catalyst layer on both the cathode and the anode sides were assumed to be isotropic with a permeability of 10^{-12} m^2.
(5) Four reactant species, viz. H_2, O_2, N_2, and H_2O (vapor) were considered.
(6) Bipolar/end plates fabricated out of SS-316 alloy were used in the development of the model.
(7) The volume of the liquid H_2O was assumed to be negligible in the domain. Due to the high thermal conductivity of metallic bipolar/end plates, it was assumed that whatever liquid water droplets are present would be only on the walls of the channels in the flow-field of these plates. Therefore, it can be assumed that there is no restriction to the flow of gases in the thin channels of the flow-field due to the presence of liquid water species.
(8) Due to pressure variation and electrochemical reactions, the density of the gaseous mixture varies from location to location in the domain. Hence, compressible gas technique (ideal gas behavior) was used to determine the density of the gas mixture at every control volume element in the domain.
(9) Gas mixture viscosity was calculated using mass-weighted-mixing-law.
(10) The species binary diffusion coefficient was calculated using kinetic theory of gases [4].
(11) Since we are using metallic bipolar/end plates (without surface modification), there is an appreciable level of contact resistance from these plates. To take these losses into account, we assume that the oxide film thickness on these plates to be constant, and that the contact resistance of the bipolar/end plates with the electrodes was a function of compaction pressure of stack.

2.3. Governing equations

The governing equations for this unified model can be divided into three different categories, viz. (1) transport equations; (2) thermodynamic equations; and (3) membrane properties equations.

2.3.1. Transport equations

These include equations of conservation of mass, momentum and species transport in the domain. These equations are implemented zone-wise in the model domain. The equation for conservation of mass in general form can be described as:

$$\frac{\partial \rho}{\partial t} + \nabla \cdot (\rho \vec{v}) = S_{\mathrm{m}} \tag{4}$$

where ρ is the density of the gaseous mixture; t the time; $\vec{v}$ the velocity vector; and S_{m} is the source term for the continuous phase. This source term corresponds to the production or consumption of reaction species in a particular zone. Since all the electrochemical reactions take place only in the cathode and anode catalyst layers, the value of S_{m} is only non-zero for these layers and is given by:

$$S_{\mathrm{m,c}} = S_{\mathrm{O_2}} + S_{\mathrm{w,c}} \tag{5}$$

$$S_{\mathrm{m,a}} = S_{\mathrm{H_2}} + S_{\mathrm{w,a}} \tag{6}$$

where the subscripts 'c' and 'a' refer to the cathode and anode sides, respectively, and S_x ($x = \mathrm{H_2}$, $\mathrm{O_2}$, w (water)) represent the source terms for species x in the catalyst layer. The density, ρ mixture is calculated using the compressible gas technique (ideal-gas behavior) and is given for multi-component system as [4]:

$$\rho = \frac{P_{\mathrm{op}} + P}{RT \sum_i \frac{m_i}{M_i}} \tag{7}$$

where P_{op} is the operating pressure; P the local relative (or gauge) pressure, m_i the mass-fraction of species i, and M_i is the molecular weight of species i.The conservation of momentum equation in general form can be described as:

$$\frac{\partial}{\partial t}(\rho \vec{v}) + \nabla.(\rho \vec{v}\vec{v}) = -\nabla P + \nabla \cdot (\bar{\bar{\tau}}) + \vec{S}_{\mathrm{p}} + S_{\mathrm{m,k}} \vec{v} \tag{8}$$

where $\bar{\bar{\tau}}$ is the stress tensor and $\vec{S}_{\mathrm{p}}$ is the momentum source term. For laminar flow through porous media, the momentum source term $\vec{S}_{\mathrm{p}}$ is proportional to velocity and is given by Darcy's law:

$$\vec{S}_{\mathrm{p}} = -\left(\frac{\mu}{\beta}\right) \vec{v} \tag{9}$$

where μ is the viscosity of the gaseous mixture given by mass-weighted mixing law:

$$\mu = \sum_i m_i \mu_i \tag{10}$$

and β is the permeability of the medium. The value of β was taken to be 10^{-12} m^2 for the electrodes and catalyst layer

The species transport equations were written in general form for each of the species H_2, O_2, N_2, and H_2O vapor. On the anode side, the species transport equations are:

$$\frac{\partial}{\partial t}(\rho m_{H_2}) + \nabla(\rho \vec{v} m_{H_2}) = -\nabla \cdot \vec{J}_{H_2} + S_{H_2} \tag{11}$$

$$\frac{\partial}{\partial t}(\rho m_{w,a}) + \nabla(\rho \vec{v} m_{w,a}) = -\nabla \cdot \vec{J}_{w,a} + S_{w,a} \tag{12}$$

and for the cathode side the species transport equations of O_2, N_2, and H_2O are:

$$\frac{\partial}{\partial t}(\rho m_{O_2}) + \nabla(\rho \vec{v} m_{O_2}) = -\nabla \cdot \vec{J}_{O_2} + S_{O_2} \tag{13}$$

$$\frac{\partial}{\partial t}(\rho m_{N_2}) + \nabla(\rho \vec{v} m_{N_2}) = -\nabla \cdot \vec{J}_{N_2} \tag{14}$$

$$\frac{\partial}{\partial t}(\rho m_{w,c}) + \nabla(\rho \vec{v} m_{w,c}) = -\nabla \cdot \vec{J}_{w,c} + S_{w,c} \tag{15}$$

where J_i is the diffusion flux of species i. The diffusion flux of species i is given by Maxwell relationship as [4]:

$$\vec{J}_i = -\sum_{j=1}^{N-1} \rho D_{i,j} \nabla m_j \tag{16}$$

where $D_{i,j}$ is the binary diffusion coefficient of species i in species j, and N is the total number of species in the mixture. The binary diffusion coefficients ($D_{i,j}$) were calculated using the kinetic theory of gases [4]. The source terms for each of the species transport equations exist only in their respective catalyst layer and are given by:

$$S_{H_2} = \left[-\frac{I(x,\ y)}{2F}\right] M_{H_2} A_{cv} \tag{17}$$

$$S_{w,a} = \left[-\frac{\alpha(x,\ y)}{F}\right] I(x,\ y) M_{H_2O} A_{cv} \tag{18}$$

$$S_{O_2} = \left[-\frac{I(x,\ y)}{4F}\right] M_{O_2} A_{cv} \tag{19}$$

$$S_{w,c} = \left[\frac{1 + 2\alpha(x,\ y)}{2F}\right] I(x,\ y) M_{H_2O} A_{cv} \tag{20}$$

where $I(x, y)$ is the local current density; F the Faradays constant; $\alpha(x, y)$ the local net water transfer coefficient per proton; and A_{cv} is the specific surface area of control volume element in the respective zone of the domain.

2.3.2. Thermodynamic equations

The Nernst equation for the H_2/O_2 fuel cell, using literature values for the standard-state entropy can be written as:

$$E = 1.229 - (8.5 \times 10^{-4})(T - 298.15) + (4.308 \times 10^{-5}) T(\ln(p^*_{H_2}) + \tfrac{1}{2}\ln(p^*_{O_2})) \tag{21}$$

where E (V) is the ideal equilibrium potential, T (K) is the cell temperature and P^*_i (atm) is the partial pressures of species i at the reaction interface. However, the actual potential of the cell decreases when the load is drawn from the cell. This is due to irreversible losses in the cell which include viz. (1) activation polarization, η_{act}; (2) ohmic polarization, η_{ohm}; and (3) concentration polarization, η_{conc}. These losses are represented by standard expressions [5] and are given in Eqs. (22)–(24).

$$\eta_{act} = \frac{RT}{F} \ln\left(\frac{I(x,\ y)}{I_0}\right) \tag{22}$$

$$\eta_{ohm} = I(x,\ y) R_{cell}(x,\ y) \tag{23}$$

$$\eta_{conc} = \frac{RT}{nF} \ln\left(1 - \frac{I(x,\ y)}{I_L(x,\ y)}\right) \tag{24}$$

where I_0 is the exchange current density; R_{cell} the ohmic resistance offered by the cell stack; and I_L the limiting current density. The actual cell voltage (V) is then, theoretical cell voltage (E) minus the polarization losses.

$$V = E - \eta_{act} - \eta_{ohm} - \eta_{conc} \tag{25}$$

The ohmic resistance, R_{cell} of the cell stack is a combination of the resistance to flow of electrons in cell components (typically bipolar plates) and the resistance to flow of ions (H^+) in the electrolyte and is given by:

$$R_{cell}(x,\ y) = R_{CR}(x,\ y) + R_{memb}(x,\ y) \tag{26}$$

where $R_{CR}(x,\ y)$ is the contact resistance of the stack and R_{memb} is the resistance offered by the electrolyte membrane to the flow of H^+ ions. The contact resistance depends upon the type of material for the bipolar/end plates and compaction force of the stack. We have shown in our previous work that metallic bipolar/end plates have several advantages over the conventionally used graphite plates [6]. Hence, we decided to develop this model using SS-316 bipolar/end plates. However, the contact resistances while using these materials (with no surface modification) can be significant due to the formation of thin oxide layer on the surface. Consequently, these contact losses should be considered in the modeling work. A relationship between compaction force and contact resistance for SS-316 was developed by curve fitting the data from Hodgson et al. [7]. The equation for contact resistance for SS-316 is given by:

$$R_{CR}^{SS316} = 2.62 F_{stk}^{-0.9231} \tag{27}$$

where R_{CR}^{SS316} is the contact resistance (Ω m^2) and F_{stk} is the compaction pressure of the stack in N m^{-2}. The resistance to

Table 1
Equations for local membrane properties [8–12]

Activity of water (a) on the membrane-electrode interface	$a_k = \frac{X_{w,k} P}{P^{sat}_{w,k}}$
Saturation vapor pressure of water at 'k' interface	$\log_{10}(P^{sat}_{w,k}) = 2.95 \times 10^{-2} T_k - 9.18 \times 10^{-5} T_k^2 + 1.44 \times 10^{-7} T_k^3 - 2.18$
Water content in membrane (k = a)	$\lambda = 0.043 + 17.81 a_k - 39.85 a_k^2 + 36 a_k^3, \quad 0 < a_k \leq 1; \qquad \lambda = 14 + 1.4(a_k - 1), \quad 1 < a_k \leq 3$
Electro-osmotic drag coefficient	$n_d = 0.0029\lambda^2 + 0.05\lambda - 3.4 \times 10^{-19}$
Diffusion coefficient of water in the membrane at temperature T_c (K)	$D_w = D_i \exp\left(2416 \times \left(\frac{1}{T_0} - \frac{1}{T_c}\right)\right), \quad T_0 = 303\,K; \qquad D_i = 10^{-10}, \quad \lambda < 2, D_i = 10^{-10}, \quad \lambda < 2; \qquad D_i = 10^{-10}, \quad (1 + 2(\lambda - 2)), \quad 2 \leq \lambda \leq 3; \qquad D_i = 10^{-10}(3 - 1.67(\lambda - 3)), \quad 3 < \lambda < 4.5; \quad D_i = 1.25 \times 10^{-10}, \quad \lambda \geq 4.5$
Water concentration at membrane-electrode interface	$C_{w,k} = \frac{\rho_{m,dry}}{M_{m,dry}}(0.043 + 17.8 a_k - 39.85 a_k^2 + 36 a_k^3) \quad a_k \leq 1$; $C_{w,k} = \frac{\rho_{m,dry}}{M_{m,dry}}(14 + 1.4(a_k - 1)) \quad a_k > 1$, $\rho_{m,dry} = 2000\,kg\,m^{-3}$, $M_{m,dry} = 1.1\,kg\,mol^{-1}$
Membrane conductivity	$\sigma_m = \left(0.514 \frac{M_{m,dry}}{\rho_{m,dry}} C_{w,a} - 0.326\right) \exp\left[1268\left(\frac{1}{T_0} - \frac{1}{T_s}\right)\right]; \quad T_0 = 303\,K, \quad T_s$ = surface temperature at anode
Net water transfer coefficient in membrane neglecting the convection term	$\alpha = n_d - \frac{F}{I}\left[D_w \frac{(C_{w,c} - C_{w,a})}{t_m}\right]$

flow of ions (H^+) in the electrolyte membrane depends on the proton conductivity of the membrane (σ_m) and the thickness of the membrane (t_m), and is given by the expression:

$$R_{memb} = \frac{t_m}{\sigma_m(x,\ y)} \tag{28}$$

2.3.3. Membrane properties equations

The water content and the flux of water in the membrane are important for current density prediction in the cell [8,9]. The equations for the electrolyte membrane properties are empirical equations and are obtained by experimental data [8–12]. Table 1 gives a compiled list of all the membrane properties equations that were used in the development of this model and the detailed explanation of these equations are given in several references [8–12]. It may be noted that all the properties referred to in this section are the local properties values on the X–Y reaction interface, and the suffix (x, y) has been taken out just for mere simplicity.

2.4. Solution strategy

The geometry of the domain was defined in Gambit® software. The geometry consists of cathode and anode flow-fields and membrane electrode assembly (MEA) sandwiched in between. For meshing the domain, hexahedron volume element with 20 nodes per element and map scheme was chosen. Total number of the volume elements with the chosen mesh size was around 0.4 million. The geometry was then exported to Fluent® 6.0 software. The formulated transport equations were solved using the simple algorithm [4] for each of the control volume element in the domain. Second order implicit method was used for unsteady-state formulation. Thermodynamic and membrane properties equations were incorporated through the use of user defined function (UDFs) codes written in C language. All the equations were solved and the parameters (membrane properties, local current density, etc.) were updated at the start of every iteration using the adjust function. A grid adaption technique was used to obtain a grid independent solution. Because of the memory and time requirements for the iteration process, the Fluent® and the Gambit® softwares were run on Dell® Precision® workstation (Intel® Xeon® 2.2 GHz, 1.5 GB SDRAM).

3. Results and discussions

Simulations were done for different flow-field designs in the bipolar/end plates of the polymer electrolyte membrane fuel cell. Temperature and pressure for all the simulations were kept constant at 350 K and 202 kPa, respectively. Reactant gases were externally humidified. On the cathode side, humidified air consisting of 21 mass% of O_2, 70.5 mass% of N_2 and 8.5 mass% of H_2O vapor was used. The anode side reactant gas consists of 40 mass% of H_2 and 60 mass% of H_2O vapor. The velocity inlets for the cathode and anode sides were 5.0 and 2.5 m s^{-1}, respectively.

The steady-state results were first obtained by de-selecting the transient option from the Fluent® software. De-selecting, essentially removes all the time dependent terms from the transport equations. The current density for these simulations was fixed at 5000 A m^{-2}. As discussed earlier, voltage level was used to judge the performance of the fuel cell. The simulated voltages for serpentine, parallel, multi-parallel and discontinuous designs were 0.66, 0.64, 0.68 and 0.71 V, respectively. These are marked by dotted lines in the steady-state region of Fig. 3. From this, we can conclude that the discontinuous type of flow-field design will perform better than the other three designs. This is because the discontinuity of the channels forces the gas into the diffusion layer, thereby making the transfer of reactant gases in the gas diffusion layer from diffusion to diffusion

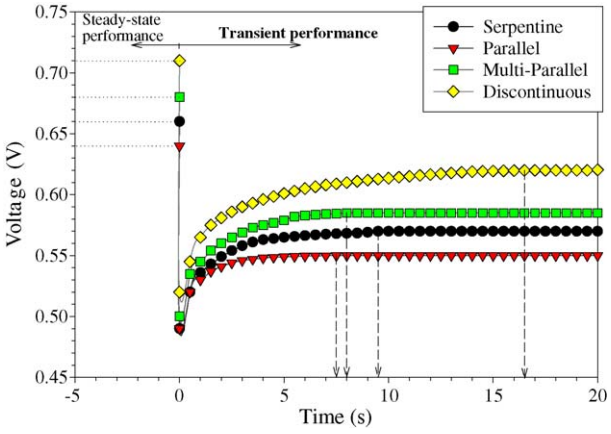

Fig. 3. Steady state and transient performance for one cell PEM fuel cell stack using different flow-field designs in the bipolar/end plates.

plus convection type. This increases the effective pressure of the reactions species at the reaction interface. These findings are consistent with those of Watkins et al. [1], who proposed the design as a solution to the problem of increased gas diffusion.

The transient response of the PEMFCS was studied by changing the load level (current) from 5000 to 8000 A m^{-2} instantaneously. The sudden load change was made at time, $t = 0$ s. It was assumed that the fuel cell has a steady state at all times, $t < 0$ s. The simulated voltage for the transient region is shown in Fig. 3. Initially when the load level is increased, the voltage suddenly drops, and then leveled off to a value slightly higher than the dropped value. The time to level off was measured from the time when the load level was suddenly increased ($t = 0$ s) to the time when the change in voltage is less than 0.1 mV. The time for the transient response for serpentine, parallel, multi-parallel and discontinuous type of flow-designs was 9.5, 7.5, 8.0, and 16.5 s, respectively. It was seen that the parallel type of design gave the best performance, while the transient performance from the discontinuous type of design was low.

As discussed above, the discontinuous type of design gives the maximum steady-state performance, but lowest transient performance. On the other hand the parallel flow-field design gave the lowest steady-state performance but highest transient performance. The multi-parallel type of flow-field design on the other hand gives reasonable good values for both the steady state and transient performance. So, with such flow-field designs in the bipolar/end plates, the overall performance characteristics of the fuel cell can be increased.

Also it is worth mentioning that the use of design also depends upon the type of applications. If the fuel cell is used for stationary applications where steady-state response is more important than the transient response, discontinuous type of flow-field design will serve as a better choice. However, if the fuel cell were used for automobile applications, where transient response is important along with the steady-state performance, it would be wise to use multi-parallel type of flow-field designs.

Also it may by noted that the voltage transient response values are in order of 0.1 V, which may appear to be insignificant. These values should be used as a caution, as this depicts the voltage variation in one cell only. In commercial cell stacks (∼100 cell or more), the voltage variations from all the cells would add up resulting in an appreciable level of transient voltage drop. The present model in our further studies would be extended to study the transient characteristics for the large fuel cell stacks. The use of such models will help in the optimization of the design process for the flow-field in the bipolar/end plates and will give the fuel cell developers a scope of further improvement of the fuel cell technology.

4. Conclusions

A unified, three-dimensional, transient numerical mass-transfer single cell model for polymer electrolyte membrane fuel cell was developed. Simulations were performed with different flow-designs in the bipolar plate. The relative performance of the different designs was judged from the voltage levels at a constant current density. The simulated steady-state voltage for discontinuous type of design at an average current density of 5000 A m^{-2} was 0.71 V, which was maximum amongst the designs chosen for simulations in this study. The transient performance of the cell was studied when the load levels were varied from 5000 to 8000 A m^{-2}. Results showed that the transient response for the parallel type of design was highest, and it took only 7.5 s for the cell to get back to steady state again. However, the steady-state voltage for parallel flow-field is comparatively lower than the other three designs. An optimized approach is therefore to choose multi-parallel design, where reasonable values of steady-state voltage at 5000 A m^{-2} and transient response are obtained. This model can be extended to calculate the steady state and transient performances of the large commercial stacks, and can help in to improve the performance characteristics of the fuel cell stack.

Acknowledgments

The authors are grateful for the support of this work by Center of Advanced Vehicle Technologies (CAVT) at the University of Alabama, which is funded by United States Department of Transport (US DOT) grant no. DTFH61-91-X-00007.

References

[1] D.S. Watkins, K.W. Dircks, D.G. Epp, US Patent No. 4988583, 1991.
[2] E. Hontanon, M.J. Escudero, C. Bautista, P.L. Garcia-Ybarra, L. Daza, Optimization of flow-field in polymer electrolyte membrane

fuel cells using computational fluid dynamics technique, J. Power Sources 86 (2000) 363–368.
[3] A. Kumar, R.G. Reddy, Effect of channel dimensions and shape in the flow-field distributor on the performance of the polymer electrolyte membrane fuel cells, J. Power Sources 113 (2003) 11–18.
[4] Fluent® 6.0 User Guide Documentation, Fluent Inc., Lebanon, New Hampshire, 2001.
[5] Fuel Cell Handbook, 5th ed., EG&G Services, Parsons, Inc., US Department of Energy Office of Fossil Energy, National Energy Technology Laboratory, West Virginia, 2000, pp. 2.4–2.8.
[6] A. Kumar, R.G. Reddy, PEM fuel cell bipolar plates – material selection, design and integration, in: P.R. Taylor (Ed.), Proceedings of the 2002 TMS Annual Meeting, TMS Warrendale, PA, 2002, pp. 41–53.
[7] D.R. Hodgson, B. May, P.L. Adcock, D.P. Davies, New light weight bipolar plate system for polymer electrolyte membrane fuel cells, J. Power Sources 96 (2001) 233–235.
[8] S. Dutta, S. Shimpalee, J.W. Van Zee, Numerical prediction of mass-exchange between cathode and anode channels in a PEM fuel cell, Int. J. Heat Mass Trans. 44 (2001) 2029–2042.
[9] T.E. Speringer, M.S. Wilson, S. Gottesfeld, Modeling and experimental diagnostics in polymer electrolyte fuel cells, J. Electrochem. Soc. 140 (1993) 3344–3513.
[10] J.S. Yi, T.V. Nguyen, An along-the-channel model for proton exchange membrane fuel cells, J. Electrochem. Soc. 145 (1998) 1149–1159.
[11] J.S. Yi, T.V. Nguyen, The effect of the flow distributor on the performance of PEM fuel cells, in: S. Gottesfeld, G. Halpert, A. Landgrebe (Eds.), Proceedings of First International Symposium on Proton Conducting Membrane Fuel Cells, vol. 95-23, The Electrochemical Society, Inc., Pennington, NJ, 1995, pp. 66–75.
[12] T.V. Nguyen, R.E. White, A water and heat management model for proton-exchange-membrane fuel cells, J. Electrochem. Soc. 140 (1993) 2178–2186.